Zinc Phthalocyanine Conjugated Dimers as Efficient Dopant-Free Hole Transporting Materials in Perovskite Solar Cells

Desiré Molina,[a, b] Marco A. Ruiz-Preciado,[c] Brian Carlsen,[b] Felix Thomas Eickemeyer,[c] Bowen Yang,[b] Natalie Flores-Díaz,[b] Maria João Álvaro-Martins,[a] Kazuteru Nonomura,[b] Anders Hagfeldt,*[b] and Ángela Sastre-Santos*[a]

Four ZnPc-dimers with 2,5-thienyl (ZnPc–th–ZnPc **1**), 2,7-fluorenyl (ZnPc–flu–ZnPc **2**), 3,6-bisthienylldiketopyrrolopyrrole (ZnPc–DPP–ZnPc **3**) and 1,4-phenyl (ZnPc–p–ZnPc **4**) bridges have been studied as dopant-free hole transporting materials (HTMs) in perovskite solar cells (PSCs). The synthesis and characterization of ZnPc–th–ZnPc **1** and ZnPc–flu–ZnPc **2** dimers are reported for the first time. Steady state and time resolved photoluminescence demonstrate the good hole-extraction capability of these materials. The best efficiencies obtained for dimers **1**, **2**, **3** and **4** are 15.5%, 15.6%, 16.8% and 15.7%, respectively, without the addition of dopants. Besides, these derivatives demonstrated better stability both in dark storage conditions with a relative humidity $<20\%$ for 500 h and at 50 °C with a relative humidity $>60\%$ for 160 h when compared to doped spiro–OMeTAD. The push-pull nature of dimer ZnPc–DPP–ZnPc **3** has led to the highest efficiency among the ZnPc derivatives under study demonstrating that donor-acceptor-donor systems can be good alternatives to commonly used materials due their energy levels, low cost and the final morphology of the hole transporting layer.

1. Introduction

Perovskite solar cells (PSCs) stand out among all third-generation solar cells due to their high efficiencies. These excellent results are as a result of the possibility of deposition via solution processing, their strong panchromatic absorption, long carrier lifetime, bipolar diffusion and tunable band gap.[1] However, long-time stability is still a challenge to overcome.[2] The best efficiencies have been obtained by sandwiching the active layer between hole and electron transporting layers (HTL and ETL, respectively). These improve the selective blocking and extraction of charges into the external circuit and also play a key role of chemical isolation of the perovskite active layer, which is affected by oxygen, moisture, heat, light and interfacial degradation, all of which can cause reduced device performance. In the regular architecture (n-i-p), the hole transporting layer is the layer which is responsible for this isolation. In this respect, the small molecule 2,2′,7,7′-tetrakis(*N*,*N*-di-*p*-methoxyphenylamine)-9,9′-spirobifluorene (Spiro–OMeTAD) and the polymer poly-(triarylamine) (PTAA) are commonly used to manufacture high efficiency n-i-p PSCs. Unfortunately, the best efficiency results are obtained with doped hole transporting materials (HTMs), where dopants negatively affect the stability. It has been observed that the use of dopants like lithium bis(trifluoromethanesulfonyl)imide (Li–TFSI) and 4-*tert*-butylpyridine (*t*BP) in HTM accelerates the cell degradation since they are hygroscopic and are able to spread to neighboring layers.[3] Moreover, the addition of dopants increases the final price of the devices.

Phthalocyanines (Pcs) are semiconductor materials known for their optoelectronic properties, such as intense absorption in the near-infrared region, excellent thermal and chemical stability, and chemical versatility.[4] Pcs are applied in photovoltaic technologies as light absorbers and sensitizers in dye-sensitized solar cells,[5] as donor materials in organic solar cells.[6] Pcs have also been included in organic-inorganic hybrid PSCs as hole transporting material.[7] In 2015, promising results were reported with vacuum-deposited CuPc as HTM in standard configuration.[8] Afterwards, Zhang and co-workers reported highly stable vacuum-deposited CuPc as HTM combining low temperature and doctor-blade technique processed carbon as a cathode material for application in a $MAPbI_3$-based perovskite solar cell (MA = methylammonium), achieving a considerably high power conversion efficiency (PCE) of 16.1%.[9] The introduction of substituents in peripheral and non-peripheral positions can give the Pcs the necessary solubility in

[a] Dr. D. Molina, M. J. Álvaro-Martins, Prof. Dr. Á. Sastre-Santos
Área de Química Orgánica, Instituto de Bioingeniería
Universidad Miguel Hernández
Avda. de la Universidad, s/n, Elche 03202 (Spain)
E-mail: asastre@umh.es
[b] Dr. D. Molina, B. Carlsen, Dr. B. Yang, N. Flores-Díaz, Dr. K. Nonomura, Prof. Dr. A. Hagfeldt
Laboratory of Photomolecular Science, Institute of Chemical Sciences and Engineering
École Polytechnique Fédérale de Lausanne
1015 – Lausanne (Switzerland)
E-mail: anders.hagfeldt@epfl.ch
[c] Dr. M. A. Ruiz-Preciado, Dr. F. T. Eickemeyer
Laboratory of Photonics and Interfaces, Institute of Chemical Sciences and Engineering
École Polytechnique Fédérale de Lausanne
1015 – Lausanne (Switzerland)

Supporting information for this article is available on the WWW under https://doi.org/10.1002/cptc.201900245

common organic solvents that allow the HTL deposition by techniques such as roll-to-roll and spin coating. In these conditions, it was possible to obtain a PCE exceeding 20% with doped copper(II) 2,9,16,23-tetra-tert-butyl-29*H*,31*H*-phthalocyanine.[10] Solution-processable CuPcs as dopant-free HTMs have also been reported, showing efficiencies between 11–15%.[11] Guo and co-workers have recently presented three new Pcs ($CuPcNO_2$–OMFPh, $CuPcNO_2$–OBFPh, $ZnPcNO_2$–OBFPh) as HTM. Of these, zinc–phthalocyanine gave the best results in both stability and efficiency (PCE = 15.74%) in a $(FAPbI_3)_{0.85}(MAPbBr_3)_{0.15}$ (FA = formamidinium) PSC.[11d] Recently, Sun *et al.* achieved the record for dopant-free HTMs based on Pcs, delivering an impressive PCE of up to 17.6% under one sun illumination with CuPc–OBu.[12] The PCE record for HTMs based on ZnPcs is in the hands of Nazeeruddin, Torres *et al.* with a maximum efficiency of 17.5% for doped tetra-5-hexylthiophene ZnPc.[13] Very recently arylamine CuPc has reached an incredible PCE of 19,7%.[14]

In a recently published paper we showed a preliminary study of a *p*-phenylene ZnPc dimer (ZnPc–p–ZnPc **4** in this work) as doped HTM in PSCs, obtaining a maximum power conversion efficiency of 15.2%, which was higher than that obtained for the non-dimer TB_4–ZnPc (2,9,16,23-tetra-*tert*-butyl-29*H*,31*H*-phthalocyanine, PCE = 14.4%).[15] These results indicated that ZnPc dimers are promising materials for this application requiring a deeper analysis of the influence of the structure of these molecules on the final performance of PSC devices.

In this work, we compare four Pc-dimers as HTMs which have different conjugated systems between the zinc tri-*tert*-butyl phthalocyanines units. These linkers are 2,5-thienyl (ZnPc–th–ZnPc **1**), 2,7-fluorenyl (ZnPc–flu–ZnPc **2**), 3,6-bisthienylldiketopyrrolopyrrole (ZnPc–DPP–ZnPc **3**) and 1,4-phenyl (ZnPc–p–ZnPc **4**) (Figure 1). On this occasion, we applied materials without dopants to overcome the drawbacks of the use of these substances. The devices, with n-i-p architecture FTO/c–TiO_2(compact)/m–TiO_2(mesoporous)/Perovskite/HTM/Au, containing the dimers as HTM are also compared with other control devices with non-doped TB_4–ZnPc and doped spiro–OMeTAD as HTMs. While the dimers ZnPc–th–ZnPc **1**, ZnPc–flu–ZnPc **2** and ZnPc–p–ZnPc **4** showed similar photovoltaic characteristics, with efficiencies between 15.5 and 15.7%, ZnPc–DPP–ZnPc dimer **3** stood out with an efficiency of 16.8%. The push-pull character of the DPP bridge could determine an adequate molecular packaging that confers the HTL a more suitable morphology for hole extraction and electron blocking. In addition, these ZnPcs-based compounds have been shown to confer more stability on devices than doped spiro–OMeTAD, both in storage conditions and under thermal and humidity stress. Our findings suggest that proper conjugated bridges could further boost the performance and stability of phthalocyanine-based perovskite solar cells.

2. Results and Discussion

2.1. Synthesis

ZnPc–th–ZnPc **1** and ZnPc–flu–ZnPc **2** were easily synthesized by Suzuki-Miyaura coupling between zinc tri-*tert*-butyl(iodo) phthalocyaninate (IZnPc) and 2,2′-(2,5-thiophenediyl)bis[4,4,5,5-tetramethyl-1,3,2-dioxaborolane or 2,2′-(9,9-dioctyl-9*H*-fluo-

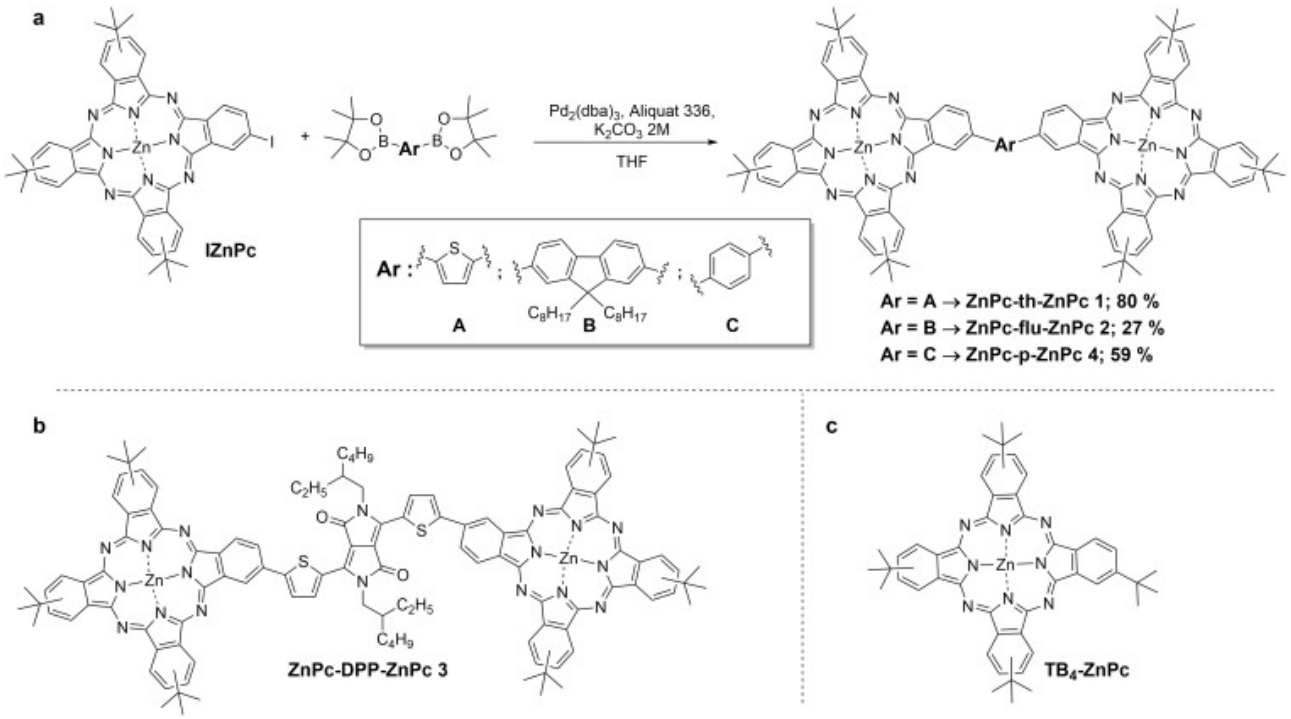

Figure 1. a) Synthesis of ZnPc–th–ZnPc **1** and chemical structure of b) the dimer ZnPc–DPP–ZnPc **3** and c the non-dimer TB_4–ZnPc.

rene-2,7-diyl)bis[4,4,5,5-tetramethyl-1,3,2-dioxaborolane in 80 and 27% yield respectively (Figure 1a). It was found that using Aliquat 336 as a phase-transfer catalyst instead of $(C_8H_{17})_4NBr$ improved the yield of the dimer **1** from 15 to 80%, although this improvement did not happen in ZnPc–flu–ZnPc **2** reaction.

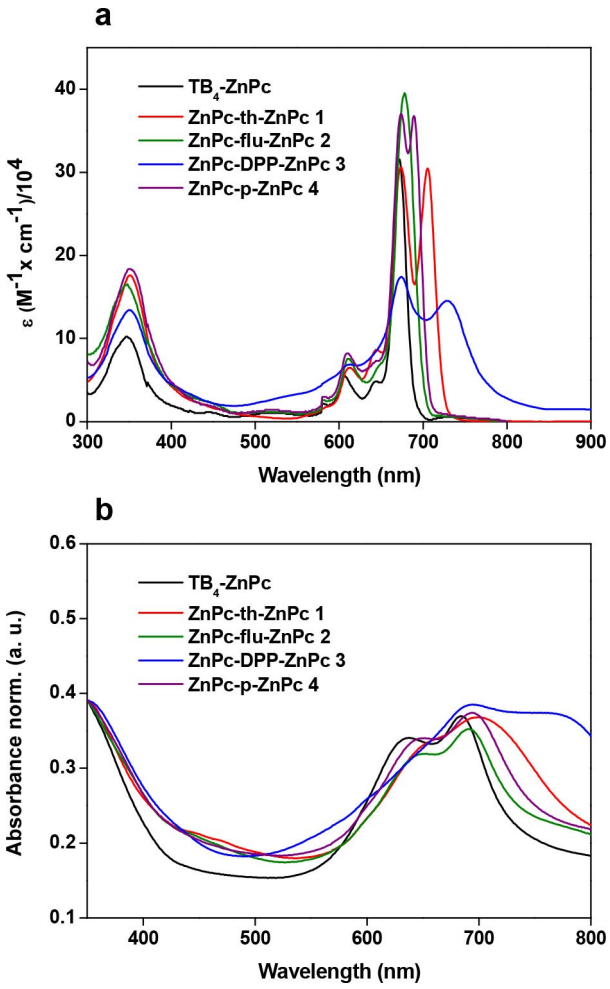

Figure 2. UV/Vis absorption spectra of TB_4–ZnPc and ZnPc dimers in a) THF solution and b) films.

Table 1. Optical and electrochemical parameters of ZnPc–th–ZnPc **1**, ZnPc–flu–ZnPc **2**, ZnPc–DPP–ZnPc **3**, ZnPc–p–ZnPc **4**, TB_4–ZnPc and spiro–OMeTAD.

HTM	λ_{abs} [nm][a]	λ_{em} [nm][b]	$E_{g,opt}$[d]/$_{EC}$ [eV][e]	HOMO [eV][f]	LUMO [eV][g]
ZnPc–th–ZnPc 1	674/705	694[b]	1.59	-4.93	-3.34
ZnPc–flu–ZnPc 2	678	–	1.74	-5.11	-3.37
ZnPc–DPP–ZnPc 3	674/729	–	1.60	-4.90	-3.30
ZnPc–p–ZnPc 4	674/689	700[b]	1.79/1.59	-4.90	-3.31
TB_4–ZnPc	672	687[c]	1.83/1.79	-5.05	-3.26
Spiro–OMeTAD[18]	–	–	2.93	-5.25	-2.32

[a] Absorption and emission spectra were measured in THF solution. [b] Excitation wavelength was 674 nm. [c] Excitation wavelength was 672 nm. [d] $E_{g,opt}$ [eV] was determined from the intersection of normalized absorption and emission spectra registered in THF. [e] $E_{g\ EC}$ [eV] was calculated by $E_{g\ EC} = E_{red1} - E_{ox1}$. [f] HOMO [eV] was calculated by HOMO = $-E_{ox1}$ (vs. Fc/Fc+)−4.8. [g] LUMO [eV] was calculated by LUMO = HOMO + $E_{g\ EC}$ [eV] (CV).

ZnPc–DPP–ZnPc **3**,[16] and ZnPc–p–ZnPc **4**[15] were prepared as previously described. These dimers are not completely soluble in halogenated solvents at room temperature, but they are very soluble in THF. The new dimers were fully characterized by ^{1}H-NMR, UV-Vis and FT-IR spectroscopies, and HR-MALDI-TOF mass spectrometry (see Supporting information).

2.2. Spectroscopic and Electrochemistry Studies

The UV-Vis absorption properties of the dimers **1**, **2**, **3** and **4** are shown in Figure 2 along with that of the non-dimer TB_4–ZnPc, all in THF solution and film. All Q band maxima of the dimers in solution and film appear bathochromically displaced and wider than that of the non-dimer due the more extended conjugation of these systems (Table 1). The Q band of dimer **1**, **3** and **4** is split in two in THF solution. This is likely caused by the presence of regioisomers and their non-symmetric character.[17] It seems that the greater the degree of stacking of the molecules, the wider the signals and the lower the molar extinction coefficient (ε). That is not the case of dimer **2**, since it seems that 9,9-dioctyl-9*H*-fluorene moiety reduces the aggregation of the molecules, showing an intense Q band at 678 nm and an ε of almost $4\times10^5\ M^{-1}cm^{-1}$. The Q band of ZnPc–DPP–ZnPc dimer **3** in solution is the widest with the smallest ε, absorbing from 500 nm to 800 nm. The latter absorbs longer wavelengths than the other dimers in solid state, exceeding 800 nm. Absorption spectra of the film on glass, seen in Figure 2b, show a widening of the signals to both red and blue if we compare them with the spectra in solution. This phenomenon can be related to the formation of aggregates, which also quenches the steady-state emission due to the proximity between molecules.

Photoluminescence (PL) obtained by exciting the respective absorbance maxima in THF solution of TB_4–ZnPc, ZnPc–th–ZnPc **1** and ZnPc–p–ZnPc **4** are shown in Figure S5. It was previously determined that PL is deactivated for dimer **3** by an energy transfer from the singlet excited state of the DPP unit to the absorption band of the Pc and the PL of the Pc units are partially deactivated by electronic transfer to the DPP unit. Here, we were also not able to detect the PL of dimer **3**, as well as of dimer **2**. We suspect that a similar process is active in dimer **2**.

Cyclic voltammetry (CV) analysis was carried out in order to know if these derivatives have suitable highest occupied molecular orbital (HOMO) and lowest unoccupied molecular orbital (LUMO) levels for triple-cation PSC (Figure S6). The redox couple ferrocene/ferricenium ion (Fc/Fc^+) was used as the external standard, and 4.8 eV below the vacuum was established as reference level. The energy positions of the HOMO and LUMO levels were estimated from the onset values for the reduction and oxidation potentials through the equations: LUMO = −|$Ered_1$ (vs. Fc/Fc^+) + 4.80| eV and HOMO = LUMO − $Eg_{\ EC}$ eV. The values of the HOMO values of the five materials (dimer **1**: −4.93 eV, dimer **2**: −5.11 eV, dimer **3**: −4.90 eV, dimer **4**: −4.90 eV, and TB_4–ZnPc: −5.05 eV) are above that of the corresponding one of the triple-cax-raytion

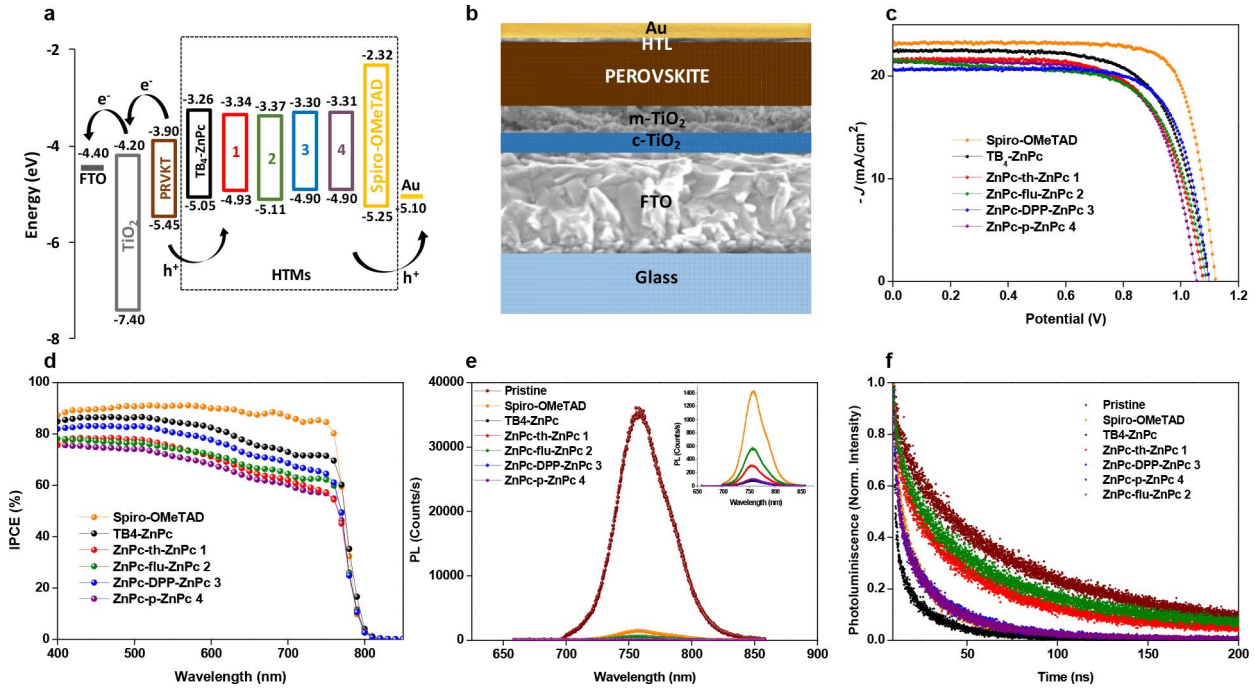

Figure 3. a) Energy level diagram for the device layers including TB_4–ZnPc, ZnPc–th–ZnPc **1** (red), ZnPc–flu–ZnPc **2** (green), ZnPc–DPP–ZnPc **3** (blue), ZnPc–p–ZnPc **4** (purple) and spiro–OMeTAD, as HTMs. b) Representation of the PSC structure with standard architecture FTO/c–TiO_2/m–TiO_2/Perovskite/HTM/Au. c) The best devices current density versus voltage (*J-V*) curves (backward measurements); d) IPCE as a function of wavelength obtained for TB_4–ZnPc, ZnPc–th–ZnPc **1**, ZnPc–flu–ZnPc **2**, ZnPc–DPP–ZnPc **3**, ZnPc–p–ZnPc **4** and spiro–OMeTAD as HTM in PSCs. e) Steady-state PL spectra of pristine–perovskite and perovskite–HTM films (Glass/Perovskite/HTM). f) Time-resolved photoluminescence decay at 754 nm obtained for all samples when exciting at 550 nm from the HTM side.

perovskite $[Cs_{0.05}(FA_{0.83}MA_{0.17})_{0.95}]Pb(I_{0.83}Br_{0.17})_3$ (HOMO ≈ 5.5 eV and LUMO ≈ −3.9 eV),[18] indicating that hole extraction would be efficient. However, lower open circuit voltages than in the case of spiro–OMeTAD can be expected because the HOMO levels are 0.32, 0.14, 0.35, 0.35 and 0.20 eV above that of the control HTM (−5.25 eV) (Figure 3a, Table 1).[15]

In order to know the conductivity of the materials in the present study, dark conductivities were measured in-plane with a channel length L = 200 μm, a channel width w = 10 mm and different film thicknesses t measured with a profilometer. The Table 2 shows the conductivities calculated as $\sigma = (\Delta I/\Delta U \cdot L/(wt))$, where $\Delta I/\Delta U$ is the slope of the measured IV curve. The conductivity of the dimers is between 2 and 6 times lower than that of spiro–OMeTAD, and that of TB_4–ZnPc is 11 times lower.

Table 2. Dark conductivities of ZnPc–th–ZnPc **1**, ZnPc–flu–ZnPc **2**, ZnPc–DPP–ZnPc **3**, ZnPc–p–ZnPc **4**, TB_4–ZnPc and Spiro–OMeTAD.

Material	Layer thickness t [nm]	Conductivity [S/cm]
ZnPc–th–ZnPc 1	20	2.8×10^{-7}
ZnPc–flu–ZnPc 2	43	1.1×10^{-7}
ZnPc–DPP–ZnPc 3	50	1.2×10^{-7}
ZnPc–p–ZnPc 4	43	1.0×10^{-7}
TB_4–ZnPc	41	5.1×10^{-8}
Spiro–OMeTAD	40	5.9×10^{-7}

2.3. Photovoltaic Performances

Hybrid triple-cation PSCs were fabricated including the different ZnPc-based dimers as dopant-free HTMs, as well as doped spiro–OMeTAD in control devices and dopant-free TB_4–ZnPc as ZnPc–HTM reference. The standard multilayer architecture was FTO/c–TiO_2/m–TiO_2/$[Cs_{0.05}(FA_{0.83}MA_{0.17})_{0.95}]Pb(I_{0.83}Br_{0.17})_3$/HTM/Au (Figure 3b). We have carried out X-Ray diffraction of different Pc based films; however, the results indicate in all the cases that we have an amorphous film. On the other hand, in order to determine which thicknesses of HTLs were the most suitable, four concentrations of ZnPc dimers were tested, 3.50, 3.74, 4.50 and 4.74 mM (Table S1). The best concentration for dimers **1**, **3** and **4** was 3.74 mM, while for **2** it was 3.50 mM. As an example, the *J*-V curves of the best devices of each concentration of ZnPc–th–ZnPc **1** (5 days after fabrication) can be seen (Figure S7). The thickness of the HTLs was estimated to be 20 nm for ZnPc–th–ZnPc **1**, ZnPc–DPP–ZnPc **3** and ZnPc–p–ZnPc **4**, approximately 15 nm for ZnPc–flu–ZnPc **2** and 180–200 nm for spiro–OMeTAD by high-magnification scanning electron microscopy (SEM) cross-sectional image (Figure S8). The topology of the HTLs was also analyzed with SEM after depositing them on the perovskite layer and the subsequent 5 nm deposition of Au to improve its electron conductivity since otherwise it is virtually transparent by this technique (Figure S9). In the studied HTLs the shape of the perovskite crystals below can be of importance, due to the thinness of the layers. The presence of some pinholes is also observed, being less evident in the

case of ZnPc–DPP–ZnPc **3**. These surface defects are attributed to the thinness of the films. More work in this regard is currently being done. The surface image of ZnPc–flu–ZnPc **2** also shows such pinholes, visible even at low magnification. The surface image of this latter HTL is compared with and without the thin layer of gold.

Current density-voltage curves were recorded under standard AM1.5G (100 mW cm^{-2}) illumination (Figure 3c). The photovoltaic parameters obtained are summarized in Table 3. Doped spiro–OMeTAD offered better photovoltaic results than the tested non-doped materials, with a short circuit current ($-J_{sc}$) of 23.3 mA cm^{-2}, an open circuit voltage (V_{oc}) of 1.12 V, a fill factor (FF) of 78.0% and a maximum PCE of 20.4%, indicating that the devices were of high quality. Remarkable results have also been obtained with non-doped TB_4–ZnPc, with a $-J_{sc}$ of 22.4 mA cm^{-2}, V_{oc} of 1.10 V, FF of 68.5% and a PCE of 16.6% for the best cell, which are the highest values for this material in literature hitherto. Devices with dimers **1**, **2** and **4** show similar results, with maximum PCE of 15.5, 15.6 and 15.7%, respectively. Undoubtedly, the material that stands out is dimer **3**, with a maximum PCE of 16.8%. Although the $-J_{sc}$ is lower (20.6 mA cm^{-2}) than that of the other ZnPc derivatives, the FF of 73.7% and the V_{oc} of 1.10 V are as high as the non-dimer, making this material the most efficient. The fundamental structural difference between the dimers under study is the bridge between phthalocyanine rings, which affects both the optoelectronic properties and self-organization in the solid state, the latter leading to a morphology of the film with peculiar and anisotropic optoelectronic properties, including hole-extraction capability.[19] The DPP core is an electron-acceptor compared to the ZnPc and the thiophene rings, so dimer **3** has a donor-acceptor-donor (D-A-D) electronic character and it has already been observed that a D-A-D configuration can help modulate energy levels, especially that of the HOMO.[20] A high hysteresis was also observed when the *J*-V curves were measured under forward bias (more than 2% for dimers **1**, **2** and **4**, 1.8% for spiro–OMeTAD, 1.6% for non-dimer and 1.3% for dimer **3**), probably due to the perovskite/HTL interface (Figure S10). Additionally, the dispersion of the photovoltaic parameters is represented in Figure S11. The parameters of the devices fabricated with spiro–OMeTAD as HTM are less dispersed than those manufactured with the ZnPc derivatives, which is especially noticeable in the case of V_{oc}.

UV-Vis measurements of FTO/c–TiO_2/m–TiO_2/Perovskite without (pristine) and with HTMs reveal that the presence of ZnPc derivatives as HTM increase the absorption of light without altering the band gap of the perovskite (Figure S12), which is not in agreement with incident photon-to-electron conversion efficiency (IPCE). IPCE spectra from devices fabricated with ZnPc–th–ZnPc **1**, ZnPc–flu–ZnPc **2**, ZnPc–DPP–ZnPc **3**, ZnPc–p–ZnPc **4**, TB_4–ZnPc and spiro–OMeTAD as HTMs are shown in Figure 3d. Dimers **1**, **2**, **3**, **4** and TB_4–ZnPc spectra have similar shape but reflect different efficiencies converting photons into electrons. IPCE of ZnPc–DPP–ZnPc **3** and TB_4–ZnPc are over 80% up to 520 nm, from which it falls progressively to 71% and 64% respectively at 750 nm. ZnPc-dimers **1**, **2** and **4** shows an IPCE under 80% up to 480 nm and drops to around 60% at 750 nm. The hypothesis to explain this trend is mentioned in a work by Nazeeruddin and co-workers,[13] who attribute this phenomenon to the fact that the fraction of current generated in the second pass of reflected light from the gold electrode is considerably reduced as a result of the strong absorption of the Pc derivative at wavelengths above 500 nm.

As mentioned above, the HOMO levels of ZnPcs and the perovskite are favorably energetically aligned so an effective hole extraction at the interface is expected. Usually, the effective transfer of holes in the heterojunction leads to a quenching of the perovskite PL.[21] Therefore, in order to study this, steady-state PL (ssPL) and time-resolved photoluminescence (TRPL) measurements comparing pristine perovskite as reference with glass/perovskite/HTM spectra (Figure 3e and 3f), were made. All HTM tested produce a strong reduction of the emission with respect to pristine perovskite in ssPL. TB_4–ZnPc, ZnPc–th–ZnPc **1**, ZnPc–flu–ZnPc **2**, ZnPc–DPP–ZnPc **3** and ZnPc–p–ZnPc **4** produce impressive PL reduction of 99.8%, 99.1%, 98.4%, 99.7% and 98.4% respectively compared with pristine devices, more dramatic than spiro–OMeTAD (96.0%). The time decays are fit with a three-component exponential model (Table S2). A fast component dominates the PL decay in the case of all HTMs compared to that of pristine perovskite film, which is two orders of magnitude slower. Compared to the other HTMs, TB_4–ZnPc exhibit the fastest time decay, although the amplitude of τ_3 is almost double than that of spiro–OMeTAD, which could explain the difference in the PCE of the devices. In general, decay times can be due to PCE differences between different ZnPc derivatives.

According to the PL data, the ability to extract holes of this ZnPc dimers is comparable and even greater than that of

Table 3. Photovoltaic parameters of PSC devices with ZnPc–th–ZnPc **1**, ZnPc–flu–ZnPc **2**, ZnPc–DPP–ZnPc **3**, ZnPc–p–ZnPc **4**, TB_4–ZnPc and Spiro–OMeTAD as HTMs.[a]

HTM	$-J_{sc}$ [mA cm^{-2}]	V_{oc} [V]	FF [%]	PCE [%]
ZnPc–th–ZnPc 1*	21.6 (19.9 ± 1.5)	1.08 (1.06 ± 0.01)	67.6 (66.6 ± 1.1)	15.5 (14.1 ± 1.1)
ZnPc–flu–ZnPc 2*	21.6 (21.1 ± 0.7)	1.09 (1.06 ± 0.02)	66.1 (63.2 ± 5.1)	15.6 (14.3 ± 1.2)
ZnPc–DPP–ZnPc 3§	20.6 (20.4 ± 0.3)	1.10 (1.09 ± 0.02)	73.8 (71.3 ± 2.2)	16.8 (16.0 ± 0.5)
ZnPc–p–ZnPc 4*	21.3 (20.9 ± 0.5)	1.06 (1.06 ± 0.01)	69.1 (67.2 ± 2.3)	15.7 (14.9 ± 0.5)
TB_4–ZnPc*	22.4 (21.4 ± 0.8)	1.10 (1.08 ± 0.02)	68.5 (68.1 ± 1.8)	16.6 (15.6 ± 1.0)
Spiro–OMeTAD*	23.3 (23.0 ± 0.3)	1.12 (1.11 ± 0.01)	78.0 (77.3 ± 0.9)	20.4 (19.7 ± 0.4)

[a] The parameters that are presented are those of the best devices of each HTM with the *average of 8 devices in brackets, §average of 6 devices in brackets; ± standard deviation.

spiro–OMeTAD, although the difference found in conductivity agrees with the results obtained.[13,22]

Two different stability tests have been performed on devices with ZnPc dimers as HTM compared to those with spiro–OMeTAD fabricated in the same batch: stability in storage conditions (shelf stability) and under thermal stress in environmental conditions of the laboratory (thermal stability). For shelf stability test, devices with different HTMs were stored in darkness with a relative humidity (RH) of less than 20% for more than 500 hours. In Figure 4 it can be seen that in the first 200 hours there is an improvement in both V_{oc} and FF, with the consequent increase in PCE for HTMs based of ZnPc, which indicates that there is a decrease in recombination phenomena in the interface, as well as in series resistance. J_{sc} experiences a more moderate improvement in all cases. On the contrary, those devices with spiro–OMeTAD as HTM evolve over time towards lower values, although J_{sc} follows a similar trend as other materials. The thermal stress test was performed by heating the devices at 50°C on a hotplate in the air with a RH over 60%. There is also an improvement in the V_{oc}, the FF and therefore in the PCE, but much faster than in storage conditions, in the first 7 hours (Figure 5). It is remarkable that devices with spiro–OMeTAD as HTM have a greater general operational deterioration in these thermal stress conditions. At any rate, if the evolution of the parameters is compared from the stabilization of them, that is, from the first 6.75 h, it is clear that non-doped ZnPc-based materials are more stable than control cells (Figure S13). During the thermal stability test there was an interval of almost 168 hours (Storage period) in which the devices were kept in storage conditions (in darkness, 25 °C and RH < 20%) for organizational reasons. After that time there was a slight decrease in the values of all the parameters, which rose again after 43 hours in thermal conditions. Hence, it seems to be an activating effect when heat is applied to those devices with ZnPc-based HTLs. Catchpole *et al.* detected a similar improvement of the photovoltaic parameters in PSC with CuPc (structurally analogous to TB_4–ZnPc) as HTM. This behavior was attributed to the fact that a positive gold doping effect is favored by heating and because the gold particles that cause shunts in the HTL cracks are rearranged with the heat treatment. A deeper study should be performed since this phenomenon also occurs in storage conditions but more slowly, so it could involve other processes, such as changes in the crystallinity and morphology of the HTLs.[10] The material that has greater stability in both conditions and is therefore the most robust is TB_4–ZnPc, although ZnPc–DPP–ZnPc **3** has presented the highest PCE values throughout the experiment.

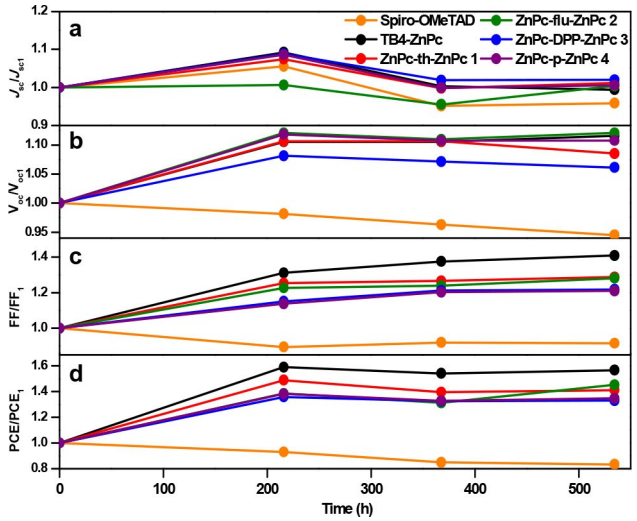

Figure 4. Shelf stability of photovoltaic parameters a) J_{sc}, b) V_{oc}, c) FF and d) PCE with HTMs ZnPc–th–ZnPc **1**, ZnPc–flu–ZnPc **2**, ZnPc–DPP–ZnPc **3**, ZnPc–p–ZnPc **4**, TB_4–ZnPc and spiro–OMeTAD.

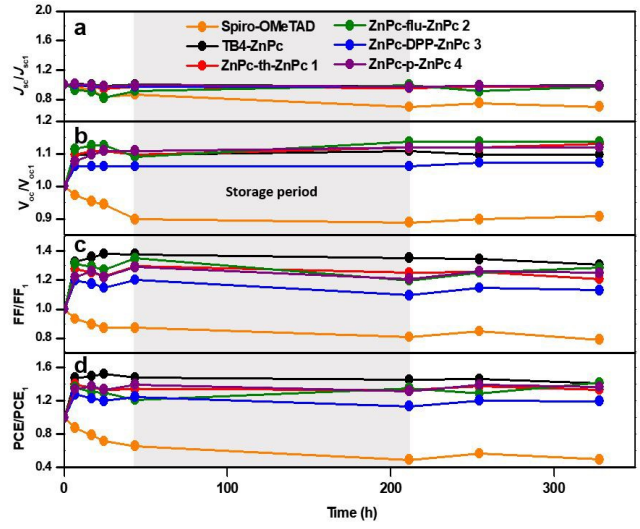

Figure 5. Thermal stability of photovoltaic parameters a) J_{sc}, b) V_{oc}, c) FF and d) PCE with different HTMs ZnPc–th–ZnPc 1, ZnPc–flu–ZnPc 2, ZnPc–DPP–ZnPc 3, ZnPc–p–ZnPc 4, TB_4–ZnPc and spiro–OMeTAD.

3. Conclusions

Two new dimers based on 2,5-thienyl-bridged ZnPc (dimer **1**) and on fluorenyl-bridged ZnPc (dimer **2**) have been synthetized and characterized. The photovoltaic performances as HTM in dopant-free PSCs of these new materials are studied by comparing them with the non-dimer TB_4–ZnPc, ZnPc–DPP–ZnPc **3** and ZnPc–p–ZnPc **4**. The devices exhibited PCE of 15.5% when using ZnPc–th–ZnPc **1**, 15.6% by using ZnPc–flu–ZnPc **2**, 15.7% for ZnPc–p–ZnPc **4** under standard global AM 1.5 illumination. Unexpectedly, a record PCE of 16.6% was reached for the non-doped reference TB_4–ZnPc, and a remarkable 16.8% PCE for ZnPc–DPP–ZnPc **3** under the same conditions of illumination. The latter shows the most reduced hysteresis behavior and less pinholes after deposition. This high PV performance gives us indications that ZnPc-dimers connected with D-A-D moieties as bridges could play a very important role in this type of photovoltaic technologies. The study of photoluminescence suggests that these dopant-free materials have a comparable hole extraction capacity and even better than doped spiro–OMeTAD. Shelf and thermal stability tests have shown that all ZnPc-based materials under study are

more stable than doped spiro–OMeTAD, highlighting the robustness of the non-dimer TB_4–ZnPc. A positive gold doping effect is favored by heating in all the HTM under study. Besides, these compounds probably are not only cheaper than spiro–OMeTAD, but they can be applied in small quantities, so the potential economic advantage is evident.

Experimental Section

Materials

All the chemicals and materials were purchased and used as received unless otherwise noted. CH_3NH_3I, CH_3NH_3Br, $HC(NH_2)_2I$ (FAI) were purchased from Dyesol and used as received. PbI_2 (99.99%) and $PbBr_2$ (99.99%) were purchased from TCI. CsI (99.9%) was purchased from Sigma-Aldrich. Chemicals for synthesis were purchased from Sigma-Aldrich and Merck, and were used without further purification unless otherwise stated. Column chromatography was performed with SiO_2 (40–63 μm), and TLC plates coated with SiO_2 60F254 were visualized by UV light.

Measurements

NMR spectrum was recorded at 25 °C with a Bruker AC300 spectrometer. The solvents for spectroscopic studies were spectroscopic grade and were used as received. UV-vis spectra in THF solution were measured with a Helios Gamma spectrophotometer and the extinction coefficients were calculated using the Lambert-Beer Law. IR spectra were measured with a Nicolet Impact 400D spectrophotometer. High-resolution mass spectra were obtained with a Bruker Microflex LRF20 matrix-assisted laser desorption/ionization time of flight (MALDI-TOF) spectrometer using dithranol as matrix. Photoluminescence (PL) measurements were recorded in Perkin Elmer LS 55 fluorometer (THF solutions) and an Andor Kymera 193i spectrometer with a 600 l/mm grating blazed at 650 nm. Samples were excited with an OBIS 660 nm CW laser (films). TRPL: TCSPC (Time-Correlated Single Photon Counting) measurements were taken using a Fluorolog 3 with a Horiba TBX-04 detector. Samples were excited with a Horiba NanoLED 637 nm pulsed laser with pulse width <200 ps (verify pulse width on laser's label).

Cyclic voltammetry measurements were performed in 0.1 M tetrabutylammonium hexafluorophosphate tetrahydrofuran solution as support electrolyte, a graphite working electrode, a Ag/Ag^+ reference electrode, and platinum counter electrode using a potentiostat/galvanostat μAutolab Type III.

Conductivity

Film thicknesses were measured with a profilometer Bruker Dektak XT and IV curve measured with a Keithley 2400.

Solar cells were measured using a 450 W xenon light source (Oriel). The spectral mismatch between AM1.5 G and the simulated illumination was reduced by using a Schott K113 Tempax filter (Präzisions Glas & Optik GmbH). The light intensity was calibrated with a Si photodiode equipped with an infrared cut-off filter (KG3, Schott), and was recorded during each measurement. The *J*-V curves were recorded in reverse bias from 1.2 to 0 V using a Keithley 2400 apparatus with scan rate being 0.125 $V s^{-1}$. The IPCE measurement was performed by an EQE system with an LED light source (Ariadne EQE) in the DC mode without any voltage bias.

The top view and cross-section SEM images characterized by a high-resolution scanning electron microscope (Zeiss Merlin) with an in-lens secondary electron detector.

Synthesis of ZnPc–th–ZnPc 1

To a degassed mixture of 2,5-bis(4,4,5,5-tetramethyl-1,3,2-dioxaborolan-2-yl)thiophene (17.3 mg, 0.05 mmol), zinc 6,16,23-tri-tert-butyl-2-iodophthalocyaninate (100 mg, 0.12 mmol), $Pd_2(dba)_3$ (5.6 mg, 0.005 mmol) and Aliquat 336 (1 drop) dissolved in THF (2.5 mL), an aqueous degassed solution of K_2CO_3 was added (2 M, 0.1 mL) under argon, then the solution was heated to 50 °C for 30 h. The crude product was purified by silica gel chromatography (hexane/dioxane 2:1) to obtain a dark green solid (65 mg, 80%). ^1H NMR (300 MHz, THF-d_8, δ, ppm): 9.57–7.91 (m, 26H, aromatic-H), 1.87–1.82 (m, 54 H, CH_3). UV-vis (THF): λ_{max}, nm (log ε) 345 (5.75), 671 (5.65). HR-MS (MALDI-TOF): m/z 1573.493 (calcd. for $[M+H]^+$ 1573.613). IR (KBr) ν_{max}, cm^{-1}: 3068, 2954, 2903, 2864, 1611, 1488, 1392, 1330, 1254, 1090.

Synthesis of ZnPc–flu–ZnPc 2

To a degassed 1,4-dioxane (2 ml) solution of 2,2′-(9,9-dioctyl-9H-fluorene-2,7-diyl)bis[4,4,5,5-tetramethyl-1,3,2-dioxaborolane (38.7 mg, 0.06 mmol), zinc 6,16,23-tri-tert-butyl-2-iodophthalocyaninate (110 mg, 0.13 mmol), $Pd_2(dba)_3$ (23 mg, 0.03 mmol), an aqueous degassed solution of K_2CO_3 (2 M, 0.12 mL) was added under argon, then the mixture was heated to 70–80 °C for 24 h. The crude product was purified by silica gel chromatography (hexane/dioxane 2:1) to obtain a dark green solid (30 mg, 27%). ^1H NMR (300 MHz, THF-d_8, δ, ppm): 9.75–9.30 (m, 15H, aromatic-H) 8.49 (m, 2 H, aromatic-H), 8.23 (m, 11H„ aromatic-H), 8.03 (m, 1 H, aromatic-H), 7.80–7.58 (m, 1 H, aromatic-H). UV-vis (THF): λ_{max}, nm (log ε) 350 (5.17), 678 (5.58). HR-MS (MALDI-TOF): m/z 1879.904 (calcd. for $[M]^+$ 1879.114). IR (KBr) ν_{max}, cm^{-1}: 3055, 2954, 2924, 2855, 1613, 1489, 1392, 1330, 1256, 1091.

Device Fabrication

First of all, FTO glass (NSG-10) was etched by a chemical method using zinc powder and HCl solution (4 M). The substrates were cleaned by 15 min sonication in four steps using HellmanexTM III (2 vol% in deionized water), deionized water, acetone, and ethanol as cleaning solvents. All substrates were cleaned by UV/ozone for 15 min before deposition. Next, compact TiO_2 layer was deposited by the spray pyrolysis method: titanium diisopropoxide acetyl acetonate (Sigma-Aldrich) was diluted in absolute ethanol and deposited on substrates at 450 °C, followed by 30 min annealing at 450 °C. Then, a mesoporous TiO_2 layer was spin coated on the compact TiO_2 (5000 rpm for 15 s with a ramp rate of 2000 rpm s^{-1}) using diluted TiO_2 paste (Dyesol 30 NR-D) in absolute ethanol. Thereafter, the substrates were annealed at 450 °C for 30 min. After cooling down the substrates to 150 °C, they were transferred to the glove box for perovskite and HTL deposition. $[Cs_{0.05}(FA_{0.87}MA_{0.13})_{0.95}]Pb(I_{0.87}Br_{0.13})_3$ mixed perovskite solution was prepared according to analogous method described by Saliba et al. for triple cation mesoporous architecture.[23] The perovskite solution was spin coated in two steps: 1) at 1000 rpm for 10 s and, 2) at 4000 rpm for 30 s. 200 μL of chlorobenzene (CB) antisolvent was dropped on top of the film 5 s before the end of the spinning during this second step. Later, the film was annealed at 100 °C for 60–80 min. HTL deposition was made after annealing. ZnPc–th–ZnPc **1**, ZnPc–DPP–ZnPc **3** and ZnPc–p–ZnPc **4** CB/THF 95:1 solutions (3.74×10^{-3} M) were spin coated at 2000 rpm for 40 s with 1000 rpm/s acceleration. ZnPc–flu–ZnPc **2** CB/THF 95:1 solution

(3.5×10^{-3} M) and TB_4–ZnPc solution (8 mg/mL CB/THF 19:1) were spin coated under the same conditions as the previous ones. Alternatively, for control devices, a 75×10^{-3} M spiro-OMeTAD CB solution, doped with Li–TFSI and *t*BP (molar ratio 0.5 and 3.3 respectively) was prepared and spin coated at 4000 rpm for 20 s with 2000 rpm s^{-1} ramp rate. Finally, 80 nm thick gold electrode was thermally deposited with an active area of 0.25 cm^2.

Acknowledgements

Á.S.S. thanks the Ministerio de Economía, Industria y Competitividad of Spain and FEDER funds by financial support (CTQ2017-87102-R). D.M. thanks the European Union through the "Programa Operativo del Fondo Social Europeo (FSE) de la Comunitat Valenciana 2014–2020". A.H. thanks Swiss National Science Foundation for financial support with the project entitled "Fundamental studies of dye-sensitized and perovskite solar cells" with project number 200020_185041. This project has received funding from the European Union's Horizon 2020 research and innovation programme under grant agreement No 764047, the "ESPResSo" project. M.A. R.-P. thanks CONACyT México for financial support through the project 291195.

Conflict of Interest

The authors declare no conflict of interest.

Keywords: hole transporting materials · perovskites · photovoltaics · phthalocyanines · solar cells

[1] a) S. Gholipour, M. Saliba, *Small* **2018**, *14*, 1802385; b) L. Lianga, Y. Caia, X. Li, M. K. Nazeeruddin, P. Gao, *Nano Energy* **2018**, *52*, 211–238; c) https://www.nrel.gov/pv/assets/images/efficiency-chart.png; d) D. Bi, X. Li, J. V. Milić, D. J. Kubicki, N. Pellet, J. Luo, T. LaGrange, P. Mettraux, L. Emsley, S. M. Zakeeruddin, M. Grätzel, *Nat. Commun.* **2018**, *9*, 4482; e) T. J. Jacobsson, J.-P. Correa-Baen, M. Pazoki, M. Saliba, K. Schenk, M. Gratzel, A. Hagfeldt, *Energy Environ. Sci.* **2016**, *9*, 1706–1724.

[2] a) R. Fu, W. Zhou, Q. Li, Y. Zhao, D. Yu, Q. Zhao, *ChemNanoMat* **2019**, *5*, 253–265; b) K. Qin, B. Dong, S. Wang, *J. Energy Chem.* **2019**, *33*, 90–99; c) C. C. Boyd, R. Cheacharoen, T. Leijtens, M. D. McGehee, *Chem. Rev.* **2019**, *119*, 3418–3451.

[3] a) J. Luo, C. Jia, Z. Wan, F. Han, B. Zhao, R. Wang, *J. Power Sources* **2017**, *342*, 886–895; b) .E. J. Juarez-Perez, M. R. Leyden, S. Wang, L. K. Ono, Z. Hawash, Y. Qi, *Chem. Mater.* **2016**, *28*, 5702–5709; c) B. Xu, J. Huang, H. Agren, L. Kloo, A. Hagfeldt, L. Sun, *ChemSusChem* **2014**, *7*, 3252–3256; d) G. Parthasarathy, C. Shen, A. Kahn, S. R. Forrest, *J. Appl. Phys.* **2001**, *89*, 4986–4992.

[4] a) S. Kong, X. Wang, L. Bai, Y. Song, F. Meng, *J. Mol. Liq.* **2019**, *288*,111012; b) J. Chena, C. Zhua, Y. Xua, P. Zhanga, T. Lianga, *Curr. Org. Chem.* **2018**, *22*, 485–504; c) K. Kadish, R. Guilard, K. Smith, in *The Porphyrin Handbook: Phthalocyanines: Spectroscopic and Electrochemical Characterization*, Academic Press, San Diego, **2003**; d) E. Ortí, J. L. Brédas, C. Clarisse, *J. Chem. Phys.* **1990**, *92*, 1228–1235; e) B. D. Berezin, in *Coordination Compounds of Prphyrins and Phthalocyanines*, John Wiley & Sons, New York, **1981**.

[5] a) P. Brogdon, H. Cheema, J. H. Delcamp, *ChemSusChem* **2018**,*11*, 86–103; b) L. Martín-Gomis, C. Parejo, J. C. Álvarez, F. Fernández-Lázaro, Á. Sastre-Santos, *Inorg. Chim. Acta* **2017**, *468*, 327–333; c) J. Suanzes-Pita, M. Urbani, G. Bottari, M. Ince, S. A. Kumar, A. Chandiran, J. H. Yum, M. Grätzel, M. K. Nazeeruddin, T. Torres, *ChemPlusChem* **2017**, *82*, 1057–1061; d) M. Urbani, M. E. Ragoussi, M. K. Nazeeruddin, T. Torres, *Coord. Chem. Rev.* **2019**, *381*, 1–64..

[6] a) F. A. Sari, M. Kazici, E. Harputlu, S. Bozar, Ö. Koyun, Y. Sahin, N. Ugur, M. Ince, S. Günes, *ChemistrySelect* **2018**, *3*, 13692–13699; b) Y. Nakata, T. Usui, Y. Nishikawa, F. Nekelson, Y. Shimizu, A. Fujii, M. Ozaki, *Jpn. J. Appl. Phys.* **2018**, *57*, 03EJ03-1–03EJ03-5.

[7] a) M. Urbani, G. de la Torre, M. K. Nazeeruddin, T. Torres, *Chem. Soc. Rev.* **2019**, *48*, 2738–2766; b) H. Lai, X. Li, S. Li, Y. Chen, B. Sun, Q. Jiang, J. Yang, *Electrochim. Acta* **2019**, *296*, 799–805; c) J. Cao, C. Li, X. Lv, X. Feng, R. Meng, Y. Wu, Y. Tang, *J. Am. Chem. Soc.* **2018**, *140*, 11577–11580; d) C. Rodríguez-Seco, L. Caba, A. Vidal-Ferran, E. Palomares, *Acc. Chem. Res.* **2018**, *51*, 869–880; e) L. Caliò, J. Follana-Berná, S. Kazim, M. Madsen, H. G. Rubahn, Á. Sastre-Santos, S. Ahmad, *Sustain. Energ. Fuels* **2017**, *1*, 2071–2077.

[8] a) C. V. Kumar, G. Sfyri, D. Raptis, E. Stathatos, P. Lianos, *RSC Adv.* **2015**, *5*, 3786–3791; b) W. Ke, D. Zhao, C. R. Grice, A. J. Cimaroli, G. Fang, Y. Yan, *J. Mater. Chem. A* **2015**, *3*, 23888–23894.

[9] F. Zhang, X. Yang, M. Cheng, W. Wang, L. Sun, *Nano Energy* **2016**, *20*, 108–116.

[10] T. Duong, J. Peng, D. Walter, J. Xiang, H. Shen, D. Chugh, M. Lockrey, D. Zhong, J. Li, K. Weber, T. P. White, K. R. Catchpole, *ACS Energy Lett.* **2018**, *3*, 2441–2448.

[11] a) Y. Wang, X. Liu, H. Shan, Q. Chen, T. Liu, X. Sun, D. Ma, Z. Zhang, J. Xu, Z.-X. Xu, *Dyes Pigm.* **2017**, *139*, 619–626; b) X. Jiang, Z. Yu, H.-B. Li, Y. Zhao, J. Qu, J. Lai, W. Ma, D. Wang, X. Yang, L. Sun, *J. Mater. Chem. A* **2017**, *5*, 17862–17866; c) J.-J. Guo, Z.-C. Bai, X.-F. Meng, M.-M. Sun, J.-H. Song, Z.-S. Shen, N. Ma, Z.-L. Chen, F. Zhang, *Sol. Energy* **2017**, *155*, 121–129; d) J. Guo, X. Meng, H. Zhu, M. Suna, Y. Wang, W. Wang, M. Xing, F. Zhang, *Org. Electron.* **2019**, *64*, 71–78.

[12] X. Jiang, D. Wang, Z. Yu, W. Ma, H. B. Li, X. Yang, F. Liu, A. Hagfeldt, L. Sun, *Adv. Energy Mater.* **2018**, 1803287.

[13] K. T. Cho, O. Trukhina, C. Roldán-Carmona, M. Ince, P. Gratia, G. Grancini, P. Gao, T. Marszalek, W. Pisula, P. Y. Reddy, T. Torres, M. K. Nazeeruddin, *Adv. Energy Mater.* **2017**, *7*, 1601733.

[14] Y. Feng, Q. Hu, E. Rezaee, M. Li, Z.-X. Xu, A. Lorenzoni, F. Mercuri, M. Muccini, *Adv. Energy Mater.* **2019**, 1901019.

[15] D. Molina, M. A. Ruiz-Preciado, F. Sadegh, M. João Álvaro-Martins, M. Grätzel, A. Hagfeldt, Á. Sastre-Santos, *J. Porphyrins Phthalocyanines* **2019**, *23*, 547–553.

[16] D. Molina, A. Guerrero, G. Garcia-Belmonte, F. Fernández-Lázaro, A. Sastre-Santos, *Eur. J. Org. Chem.* **2014**, 4585–4591.

[17] a) H. Ali, J. E. van Lier, *Tetrahedron Lett.* **2014**, *55*, 4163–4167; b) K. Kadish, R. Guilard, K. M. Smith (Eds.) *The Porphyrin Handbook. Phthalocyanines: Properties and Materials.* **2003**.

[18] Y. H. Chiang, H. H. Chou, W. T. Cheng, Y. R. Li, C. Y. Yeh, P. Chen, *ACS Energy Lett.* **2018**, *3*, 1620–1626.

[19] a) A. C. Cruickshank, C. J. Dotzler, S. Din, S. Heutz, M. F. Toney, M. P. Ryan, *J. Am. Chem. Soc.* **2012**, *134*, 14302; b) P. Gargiani, A. Calabrese, C. Mariani, M. G. Betti, *J. Phys. Chem. C* **2010**, *114*, 12258; c) F. J. Ramos, M. Ince, M. Urbani, A. Abate, M. Grätzel, S. Ahmad, T. Torres, M. K. Nazeeruddin, *Dalton Trans.* **2015**, *44*, 10847; d) W. J. Pietro, T. J. Marks, M. A. Ratner, *J. Am. Chem. Soc.* **1985**, *107*, 5387.

[20] a) P. Xu, P. Liu, Y. Li, B. Xu, L. Kloo, L. Sun, Y. Hua, *ACS Appl. Mater. Interfaces*, **2018**, *10*, 19697–19703; b) H. Zhang, Y. Wu, W. Zhang, E. Li, C. Shen, H. Jiang, H. Tian, W.-H. Zhu, *Chem. Sci.* **2018**, *9*, 5919–5928.

[21] G. Grancini, D. Viola, Y. Lee, M. Saliba, S. Paek, K. T. Cho, S. Orlandi, M. Cavazzini, F. Fungo, M. I. Hossain, A. Belaidi, N. Tabet, G. Pozzi, G. Cerullo, M. K. Nazeeruddin, *ChemPhysChem.* **2017**, *18*, 2381–2389.

[22] K. Rakstys, A. Abate, M. I. Dar, P. Gao, V. Jankauskas, G. Jacopin, E. Kamarauskas, S. Kazim, S. Ahmad, M. Grätzel, M. K. Nazeeruddin, *J. Am. Chem. Soc.* **2015**, *137*, 16172–16178.

[23] M. Saliba, J. P. Correa-Baena, C. M. Wolff, M. Stolterfoht, N. Phung, S. Albrecht, D. Neher, A. Abate, *Chem. Mater.* **2018**, *30*, 4193–4201.

Manuscript received: October 9, 2019
Revised manuscript received: December 24, 2019
Accepted manuscript online: January 12, 2020
Version of record online: February 3, 2020

After publication of the Version of Record, the figures which were originally reproduced with low resolution were exchanged with higher-resolution versions. The Supporting Information file has also been exchanged. – The Editors